Engineering Conferences International
ECI Digital Archives

5th International Conference on Porous Media and Their Applications in Science, Engineering and Industry

Refereed Proceedings

Summer 6-24-2014

# A model for magnetic drug targeting in a permeable microvessel with spherical porous carrier particles

Precious Sibanda
*University of KwaZulu-Natal*

Sachin Shaw
*University of KwaZulu-Natal*

**Proceedings of the 5th International Conference on Porous Media and its Applications in Science and Engineering**
**ICPM5**
**June 22-27, 2014, Kona, Hawaii**

# A MODEL FOR MAGNETIC DRUG TARGETING IN A PERMEABLE MICROVESSEL WITH SPHERICAL POROUS CARRIER PARTICLES

**Precious Sibanda and Sachin Shaw**

*School of Mathematics, Statistics and Computer Science, University of KwaZulu-Natal, Private Bag X01, Scottsville, Pietermaritzburg,3209,South Africa*

## ABSTRACT

We present a mathematical model for targeting a drug at malignant tissue cells in a permeable microvessel. The drug molecules are transported in carrier particles which are assumed to be porous spheres. This mode of drug delivery is non-invasive and has less toxic effects on healthy cells and tissues. The microvessel tube (see Figure 1) is subdivided into three regions, the outer endothelial glycocalyx layer where the blood has a Newtonian character, and a core and plug regions where the blood flow is described using a non-Newtonian Casson fluid model which is suitable for microvessels of radius $5\,\mu\mathrm{m}$. Targeting is achieved through a locally applied magnetic field using a cylindrical magnet positioned outside the body near the tumour position so that the carrier particles, bound with nanoparticles and drug molecules are captured at the tumour site. The study seeks to understand, *inter alia*, the effects of the size and permeability of the carrier particle, the volume fraction of embedded magnetic nanoparticles and the placement of the external magnetic field on the magnetic targeting of the carrier particles.

## INTRODUCTION

Blood flow in microvessels has different characteristics compared to blood flow through large vessels. The microscopic properties of the blood and interactions among plasma, cells and blood vessels, in particular blood-vessel wall interactions affect the nature of the blood flow through micro vessels. Due to deformation and rotation of red blood cells (RBCs), these cells accumulate near the axis of the microvessel producing a layer that moves with a constant velocity. A cell-depleted layer appears at the outer region, near the wall of the microvessel. In micro vessels or channels, blood flow represents a remarkable two-phase nature, with a peripheral layer of plasma (Newtonian fluid) and a core region of suspensions of erythrocytes which has a non-Newtonian character, Bugliarello and Sevilla [1]. Seshadri and Jaffrin [2] considered a two phase fluid model in which the outer cell-depleted layer has a lower hematocrit than the core region. The concentration of RBCs in the cell- depleted layer was assumed to be 50% of that in the core region. Gupta et al. [3] divided the outer layer into a cell-free plasma layer and cell-depleted layer. Sankar and Lee [4] investigated a two-phase fluid flow through a stenosed blood vessel. The endothelium layer of the microvessels covered by a glycocalyx layer contains a gel like layer of membrane-bound glycoproteins and plasma proteins. Liu and Yang [5] studied the eloctrokinetic effect of the endothelial glycocalyx layer in small blood vessels. The influence of the glycocalyx layer on the blood flow has been studied by many researchers, see [6, 7]. Shaw and Murthy [8] considered a two-phase fluid model and studied the significant effect of the glycocalyx layer on the magnetic targeting of a carrier particle in an impermeable microvessel. It was observed that the glycocalyx layer caused additional resistance to micro-vessel flow [9]. This was assumed to be due to its high negative charge.

A magnetic targeted drug delivery system is an attractive delivery strategy due to its non-invasiveness, high targeting efficiency and minimal toxic side effects on healthy cells and tissues [10, 11]. Mathematicals models for predicting the magnetic targeting of multifunctional carrier particles designed to deliver therapeutic agents to malignant tissue in vivo have been studied in [12]. Recently, a number of studies on magnetic drug targeting in a microvessel have used a two-phase non-Newtonian fluid model [13, 14].

Porous spheres have several, extremely valuable therapeutic and biotechnological applications, including cell immobilization, drug delivery, and as packing material in chromatography [15]. Porosity is important in improving the performance of spheres [16]. Large pores increases the permeability of the spheres, significantly increasing their surface area, allowing them to be used as culture systems for growing adherent cells, to be used for water remediation at high diffusion rates, or be used in the separation of large biomolecules, etc. [17].

The purpose of the present investigation is to explore the effect of a porous carrier particle on magnetic drug targeting in permeable microvessel using a two-phase fluid model. In the peripheral layer, the blood has a

Newtonian character while in the core and plug regions the blood can be described using the Casson model. The fluid velocity in the microvessel with a porous glycocalyx layer is presented and the trajectories of the carrier particle are analyzed for various parameters such as the permeability of the carrier particle, the radius of the carrier particle, permeability of the inner microvessel wall, distance of the carrier particle from the magnet axis, the volume fraction of nanoparticles, etc. This study will help in the understanding of the dynamics of magnetic drug targeting in a microvessel.

## NOMENCLATURE

| | | |
|---|---|---|
| h | = | Radius of the microvessel |
| $h_p$ | = | Radius of plug region |
| $J_0$ | = | Bessel function of order 0 |
| $J_1$ | = | Bessel function of order 1 |
| K | = | permeability |
| Ms | = | Magnetization of the magnet |
| N | = | number |
| R | = | Radius |
| r | = | radial coordinate |
| u | = | velocity of the fluid |
| V | = | volume |
| v | = | velocity of fluid inside the sphere |
| $Y_0$ | = | First kind Bessel function of order 0 |
| $Y_1$ | = | First kind Bessel function of order 1 |
| z | = | axial coordinate |

*Greek Symbols*

| | | |
|---|---|---|
| $\beta_{vf}$ | = | Volume fraction of nanoparticle |
| $\eta$ | = | viscosity |
| θ | = | angular coordinate |
| ε | = | permittivity of the medium |
| κ | = | Debye length |
| $\rho_e$ | = | total charge density |
| χ | = | permittivity |
| $\psi_z$ | = | Surface potential |
| τ | = | Shear stress |
| $\tau_y$ | = | Yield stress |

*Subscripts*

| | | |
|---|---|---|
| avg | = | average |
| cp | = | Carrier particle |
| g | = | Glycocalyx layer |
| mag | = | Magnet |
| mp | = | magnetic particle |
| p | = | Plug region |
| 1 | = | Fluid Region |
| 2 | = | Peripheral region |

## 1 Mathematical Formulation

Consider the microvessel as a straight circular cylinder of length $l_v$, and radius $h$. The blood flow in the micro vessel is described by a two phase non-Newtonian model. In the core region, which is of radius $h_1$, we use a Casson fluid model. The radius of the thin plug region is $h_p$. The peripheral layer of plasma near the wall is taken as a Newtonian fluid and has thickness $h - h_1$ (Figure 1). Let $(r, \theta, z)$ be the cylindrical polar coordinate system, where the z-axis is taken along the axis of the blood vessel, $r$ and $\theta$ are coordinates taken along the radial and the circumferential directions, respectively.

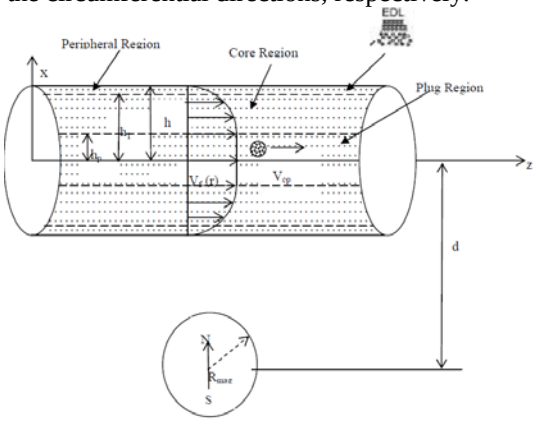


Figure 1: Schematic diagram of the problem

The fluid equations outside the sphere are written as

$$\frac{\partial u_p}{\partial r} = 0 \qquad 0 \le r \le h_p$$

$$\frac{dp}{dz} = -\frac{1}{r}\frac{\partial}{\partial r}\left\{ r\left[\left(-\mu_2 \frac{\partial u_1}{\partial r}\right)^{1/2} + \tau_y^{1/2}\right]^2\right\}$$

$$h_p \le r \le h_1 \text{ and } \tau > \tau_y \quad \textbf{(1)}$$

$$\frac{dp}{dz} = \frac{\mu_2}{r}\frac{\partial}{\partial r}\left(r\frac{\partial u_2}{\partial r}\right) + \rho_e E_z - K_g u_2$$

$$h_1 \le r \le h \text{ and } \tau_y = 0$$

and the equations inside the sphere are

$$\frac{dp}{dz} = -\frac{1}{r}\frac{\partial}{\partial r}\left\{ r\left[\left(-\mu_2 \frac{\partial v_1}{\partial r}\right)^{1/2} + \tau_y^{1/2}\right]^2\right\} - K_p v_1,$$

$$h_p \le r \le h_1 \text{ and } \tau > \tau_y, \quad \textbf{(2)}$$

$$\frac{dp}{dz} = \frac{\mu_2}{r}\frac{\partial}{\partial r}\left(r\frac{\partial v_2}{\partial r}\right) + \rho_e E_z - K_{gp} v_2,$$

$$h_1 \le r \le h \text{ and } \tau_y = 0,$$

where $\rho_e = \dfrac{\varepsilon \kappa \psi_s}{I_0(\kappa h)} I_0(\kappa r)$ is the total charge density.

The corresponding boundary conditions for the fluid

$$u_p = u_1 \qquad \text{at } r = h_p$$

$$u_1 = u_2 \text{ and } \tau_1 = \tau_2 \qquad \text{at } r = h_1 \qquad \textbf{(3)}$$

$$u_2 = 0 \qquad \text{at } r = h$$

and at the porous sphere surface

$$u_i = v_i,\ \frac{\partial u_i}{\partial r} = \mu_i\left(\frac{\partial v_i}{\partial r} - \gamma v_i\right)\ i = 1,2 \ \text{at}\ r = R \quad \textbf{(4)}$$

where *i*=1 and 2 represent the fluid region and peripheral region, respectively. Solving equations (1) with conditions (3), the velocity of the fluid at fluid region and at the porous region, respectively is written as

$$u_1(r) = \frac{1}{2\mu_1}\frac{dp}{dz}\left(\frac{4}{3}\sqrt{h_p r^3} - \frac{r^2}{2} + h_p\, r + A_1\right)$$

$$u_2(r) = A_2\, \mathrm{Y}_0\left(r\sqrt{K_g}\right) + A_3\, \mathrm{J}_0\left(r\sqrt{K_g}\right) - \frac{K_g}{\mu_2}\frac{dp}{dz} + \frac{\pi r F_0}{\mu_2(\kappa^2 - 1/K_g)\sqrt{K_g}}\mathrm{I}_0(\kappa r)$$

$$\left[\mathrm{J}_0\left(r\sqrt{K_g}\right)\mathrm{Y}_1\left(r\sqrt{K_g}\right) - \mathrm{Y}_0\left(r\sqrt{K_g}\right)\mathrm{J}_1\left(r\sqrt{K_g}\right)\right],$$

Similarly by solving equation (2) with boundary conditions (4), the velocity of the fluid inside the porous sphere in the fluid region and peripheral regions, respectively is written as

$$v_1(r) = \frac{2\sqrt{A_4\,\tau_y}}{\mu_1}\int\sqrt{\mathrm{J}_1\left(r\sqrt{K_g}\right)}dr + \frac{A_4}{\mu_1\sqrt{K_p}}\mathrm{J}_0\left(r\sqrt{K_g}\right) - \tau_y r + A_5,$$

$$v_2(r) = A_6\, \mathrm{J}_0\left(r\sqrt{K_{gp}}\right) + A_3\, \mathrm{Y}_0\left(r\sqrt{K_{gp}}\right) - \frac{K_{gp}}{\mu_2}\frac{dp}{dz} + \frac{\pi r F_0\sqrt{K_{gp}}}{\mu_2(\kappa^2 - K_{gp})}\mathrm{I}_0(\kappa r),$$

$$\left[\mathrm{J}_0\left(r\sqrt{K_{gp}}\right)\mathrm{Y}_1\left(r\sqrt{K_{gp}}\right) - \mathrm{Y}_0\left(r\sqrt{K_{gp}}\right)\mathrm{J}_1\left(r\sqrt{K_{gp}}\right)\right]$$

where the constants $A_i (i = 1,.,6)$ are given in the Appendix. The average velocity of the porous sphere carrier particle is

$$u_{avg} = 2\left(\int_0^{h_1}(u_1 - v_1)\, r\, dr + \int_{h_1}^{h}(u_2 - v_2)\, r\, dr\right)/h^2 \quad \textbf{(5)}$$

The drag force on the spherical carrier particle in Casson fluid is

$$F_f = -12\,\pi\,\eta\, R_{cp}^2\left[\left(\frac{\tau_y}{\eta}\right)^{1/2} + \left(\frac{u_{avg}}{2R_{cp}}\right)^{1/2}\right]^2, \quad \textbf{(6)}$$

The total magnetic force on the carrier particle is the sum of the forces on the embedded magnetic particles given by,

$$\mathbf{F}_m = \mu_0\, N_{mp}\, V_{mp}\frac{3\chi_{mp}}{(\chi_{mp} + 3)}(\mathbf{H}_a.\nabla)\mathbf{H}_a, \quad \textbf{(7)}$$

Following Shaw et al. [5], we obtain the radial trajectory $r(t)$ of the particle as

$$r(t) = r_0 + 2\,R_{cp}\int_{t_0}^{t}\left[\left(\frac{\mu_0\,\beta_{vf}\,R_{cp}\,M_s^2\,R_{mag}^4}{6\eta}\right)^{1/2}\frac{d^{1/2}}{\left[d^2 + (z_0 + u_{avg}\,t)^2\right]^{3/2}} - \left(\frac{\tau_y}{\eta}\right)^{1/2}\right]^2 dt \quad \textbf{(8)}$$

The axial position of the carrier particle is given by

$$z = z_0 + u_{avg}t \quad \textbf{(9)}$$

## 2 Solution Method

It is important to note that the susceptibility of the suspending medium has a significant effect on the magnetic force and also on the trajectories of the carrier particle. The nanoparticles that are used in the carrier particles are $Fe_3O_4$ particles and these are biocompatible with a density 5000kg/m$^3$.

We adopt a magnetization model for $Fe_3O_4$ and the diameter of the magnet used is 6 cm ( $R_{mag}$ = 3 cm), with a magnetization $M_s$ = $10^6$ A/m. The surface of the magnet is positioned at a distance 2.5 cm (i.e. $d$ = 5.5 cm) from the axis of the micro vessel as shown in Figure 1. This distance is altered to take into account the effect of withdrawal of the external magnetic field on the particle trajectories, which gives good information regarding the positioning of the external magnetic field. The values of the parameters have been chosen from empirical data in the literature. In particular, the following values are considered in the present study: $dp/dz = 2\times10^4$ N/m$^2$, $\psi_s = 50$ mV, $\tau_y = 4\times10^{-3}$ N/m$^2$, $e = 1.6\times10^{-19}\,C$, $h_2 = 0.985h$ $\varepsilon = 5.3\times10^{-8}\,CV^{-1}m^{-1}$, , $E_z$=5 mV, $n_\infty$=100 mol m$^{-3}$, $k_B = 1.38\times10^{-23}$ JK$^{-1}$, $z_s$=1, $D = 1.38\times10^{-10}$ m$^2$ s$^{-1}$, $h_1 = \xi_c \times h_2$, $T$ = 300 K [5].

It is worth noting that if $h_2 = h$, we retrieve the single phase fluid results.

## 3 Results and Discussion

We solved equations (8) and (9) simultaneously to determine the trajectory of the carrier particles for different parameters. The gel-like glycocalyx layer plays a vital role in blood flow as it protects the vasculature from harmful diseases such as atherosclerosis. The permeability of the glycocalyx layer influences the velocity in the outer region. The permeability of the diseased portion of a microvessel is less than that of a normal microvessel. The influence of the permeability of the glycocalyx layer on the trajectories of carrier

particles is shown in Fig. 2. From the equation(1), it is clear that this mainly affects the velocity at the cell-depleted layer. The fluid velocity decreases in the presence of a glycocalyx layer and decreases with an increase in the permeability of the layer. With a decrease in the axial velocity, the relative velocity of the carrier particle decreases and the carrier particle is easily captured at the tumour position. The drug particles are more easily captured at the tumor location than at any other location, and this is because the permeability in the tumor region is higher than in normal tissue.

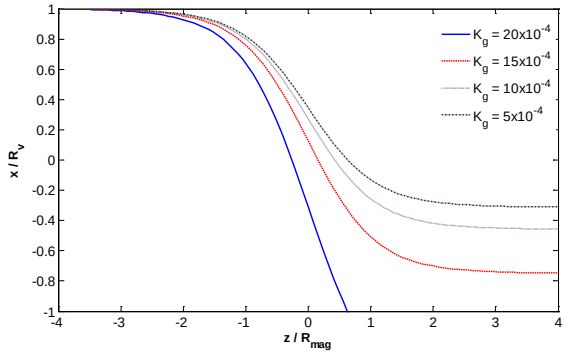


Figure 2: Trajectories of the carrier particles for different permeability of glycocalyx layer

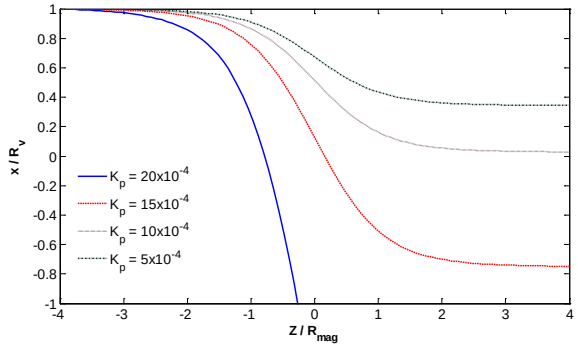


Figure 3: Trajectories of the carrier particle for different permeability of porous sphere

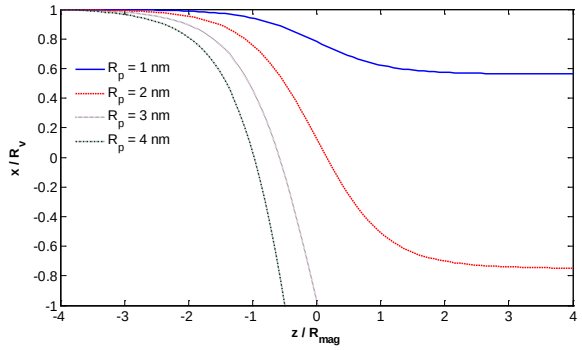


Figure 4: Trajectories of the carrier particle for different radius of the carrier particle

The magnetic force depends on the surface area of the particles. For a constant volume, the surface area of a porous sphere is larger than the surface area of a solid sphere. This is very useful for drug targeting of a tumour location. Due to porosity, the relative velocity of the porous sphere in the fluid flow is less than the fluid velocity at the microvessel. The permeability of the porous sphere plays a vital role of reducing the relative velocity of the carrier particle and increasing the magnetic force on the carrier particle. Therefore the magnetic force on the particle increases with an increase in the permeability of glycocalyx layer allowing the carrier particle to be easily captured at the tumour position.

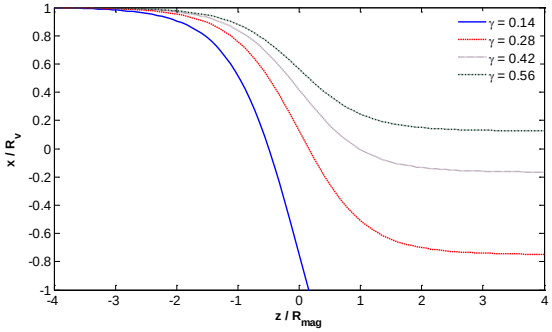


Figure 5: Trajectories of the carrier particle for difference stress-jump constants

Increasing the volume and surface area of the carrier particle increases the magnetic force on the carrier particle. As a result the magnetic force is larger and the carrier particle is easily captured at the tumour region.
From equation (4) it is clear that the stress-jump parameter reduces the fluid velocity at the sphere surface. As a result, the relative velocity of the porous sphere increases. So with an increase in the stress-jump parameter, the carrier particle moves away from the tumor region which as is clearly shown in Figure 5. For higher values, the particles are captured easily near the tumor region.

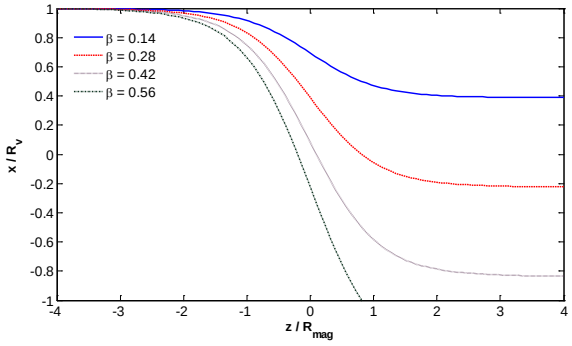


Figure 6: Trajectories of the carrier particle for different volume fraction of the nanoparticle.

From the definition, it is clear that the volume as well as the surface area of the carrier particle increases with an increase in the volume fraction of the nanoparticles. With increase in the volume fraction, the carrier particles are captured easily near the tumour position.

**Appendix**

$$N_1 = -\frac{\pi h F_0 \sqrt{K_g}}{\mu_2(\kappa^{-1}K_g)} I_0(\kappa \mathrm{h})\Big[ \mathrm{J}_0\left(h\sqrt{K_{gp}}\right) \mathrm{Y}_1\left(h\sqrt{K_{gp}}\right) - \mathrm{Y}_0\left(h\sqrt{K_{gp}}\right)\mathrm{J}_1\left(h\sqrt{K_{gp}}\right)\Big]$$

$$N_2 = \frac{\pi h_1 F_0 \sqrt{K_g}}{\mu_2(\kappa^2 - K_g)} I_0(\kappa \mathrm{h}_1)\Big[ \mathrm{J}_0\left(h_1\sqrt{K_{gp}}\right) \mathrm{Y}_1\left(h_1\sqrt{K_{gp}}\right) - \mathrm{Y}_0\left(h_1\sqrt{K_{gp}}\right)\mathrm{J}_1\left(h_1\sqrt{K_{gp}}\right)\Big]$$

$$N_3 = \frac{\pi F_0 \sqrt{K_g}}{(\kappa^{-1}K_g)}\left(I_0(\kappa \mathrm{h}_1) + \kappa I_0(\kappa \mathrm{h}_1)\right)$$

$$\Big[ \mathrm{J}_0\left(h_1\sqrt{K_{gp}}\right) \mathrm{Y}_1\left(h_1\sqrt{K_{gp}}\right) - \mathrm{Y}_0\left(h_1\sqrt{K_{gp}}\right)\mathrm{J}_1\left(h_1\sqrt{K_{gp}}\right)\Big]$$

$$+\frac{\pi h_1 F_0 K_g}{(\kappa^2 - K_g)} I_0(\kappa \mathrm{h}_1)\Big[ \mathrm{J}_0\left(h_1\sqrt{K_{gp}}\right) \left\{ \mathrm{Y}_0\left(h_1\sqrt{K_{gp}}\right) - \frac{1}{h_1\sqrt{K_{gp}}} \mathrm{Y}_1\left(h_1\sqrt{K_{gp}}\right)\right\}$$

$$-\mathrm{Y}_0\left(h_1\sqrt{K_{gp}}\right)\left\{ \mathrm{J}_0\left(h_1\sqrt{K_{gp}}\right) - \frac{1}{h_1\sqrt{K_{gp}}} \mathrm{J}_1\left(h_1\sqrt{K_{gp}}\right)\right\}\Big]$$

$$N_4 = -\mu_2\sqrt{K_g}\Big[ \mathrm{J}_0\left(h\sqrt{K_g}\right) \mathrm{Y}_1\left(h\sqrt{K_g}\right) - \mathrm{Y}_0\left(h\sqrt{K_g}\right)\mathrm{J}_1\left(h\sqrt{K_g}\right)\Big]$$

$$N_5 = \left[ \frac{1}{\sqrt{K_g}} \mathrm{Y}_1\left(h\sqrt{K_g}\right) + \frac{h_1}{2} \mathrm{Y}_0\left(h\sqrt{K_g}\right)\right] / N_4$$

$$N_6 = \left[ \mu_2\sqrt{K_g} M_1 \mathrm{Y}_1\left(h_1\sqrt{K_g}\right) - M_3 \mathrm{Y}_0\left(h\sqrt{K_g}\right)\right] / N_4$$

$$A_1 = N_5 \frac{dp}{dz} + N_6$$

$$A_2 = \left[ \frac{K_g}{\mu_2}\frac{dp}{dz} + M_1 - A_3 \mathrm{J}_0\left(h\sqrt{K_g}\right)\right] / \mathrm{Y}_0\left(h\sqrt{K_g}\right)$$

$$A_1 = -\left( \frac{4}{3}\sqrt{h_p} h_1^2 - \frac{h_1^2}{2} + h_p h_1\right) - \frac{2\mu_1}{\mu_2 K_g}$$

$$+\frac{2\mu_2}{dp/dz}\left( A_2 \mathrm{Y}_0\left(h_1\sqrt{K_{gp}}\right) + A_3 \mathrm{J}_0\left(h_1\sqrt{K_{gp}}\right) + N_2\right)$$

## CONCLUSIONS

We present the following important conclusions from this study. We have shown, inter alia, that (1) due to a larger surface area, porous particles are captured more easily at the tumour position than solid spheres, (2) the escape velocity of the carrier particles decreases when the radius of the carrier particle increases, and (3) an increase in the nanoparticle volume fraction improved the chances of the carrier particle being captured by the magnet.

## ACKNOWLEDGEMENT

The authors wish to acknowledge financial support from the National Research Foundation (NRF) and the University of KwaZulu-Natal.

## REFERENCES

[1] G. Bugliarello, J. Sevilla, Velocity distribution and other characteristics of steady and pulsatile blood flow in fine glass tubes. Biorheology 7 (1970) 85-107.

[2] V. Seshadri, M.Y. Jaffrin, Anomalous effects in blood flow through narrow tubes: a model. INSERM-Eutomech. 92 (1977) 265-282.

[3] B.B. Gupta, K.M. Nigam, M. Y. Jaffrin, three-layer semi-empirical model for flow of blood and other particulate suspensions through narrow tubes. J Biomech. Engng. 104, 129-135, 1982.

[4] D.S. Sankar, U. Lee, Two-phase non-linear model for the blood flow through stenosed blood vessels. J Mech. Sc. and Tech. 21, 678-689, 2007.

[5] Liu, M. and Yang, J. Electrokinetic effect of the endothelial glycocalyx layer on two-phase blood flow in small blood vessel, Microvas. Res., 78 (2009), 14-19.

[6] Sugihara-seki, M and Fu, B. M. Blood flow and permeability in micro vessels. Fluid Dynamics Research 37, 82-132, 2005.

[7] Potter, D. R. and Damiano, E. R. The hydrodynamically relevant endothelial cell glycocalyx observed in vivo is absent in vitro. Circ. Res. 102, 770-776, 2008.

[8] S. Shaw, P.V.S.N.Murthy, S.C.Pradhan, J Magn. Magn. Mater., 322 (2010) 1037–1043

[9] Pries, A. R., Secomb, T. W. and Gaehtgens, P. The endothelial surface layer, Eur. J. Physiol. 440, 653-666, 2000

[10] A.S. Lübbe, C. Bergeman, H. Riess, F. Schriever, P. Reichardt, K. Possinger, M. Matthias, B. Dorken, R. Gurtler, P. Hohenberger, N. Haas, R. Sohr, B. Sander, A. Lemke, D. Ohlendorf, W. Huhnt, D. Huhn, Cancer Res., 56 (1996) 4686-4693.

[11] S. Lübbe, C. Alexiou, C. Bergemann, J Surgical Res., 95 (2001) 200-206.

[12] E.J. Furlani, E.P. Furlani, J. Magn. Magn. Mater, 312 (2007) 187-193.
[13] S. Shaw, P.V.S.N. Murthy, Microvas. Res., 80 (2010) 209–220
[14] S. Shaw, P.V.S.N. Murthy and P. Sibanda, Microvas. Res., 85(2013), 77-85.
[15] H. Kim, H. Park, J. Lee, T.H. Kim, E.S. Lee, Biomaterials, 32(2011)1685–1693.
[16] S. Guven, A. Mehrkens, F. Saxer, Biomaterials, 32(2011)5801–5809.
[17] Yang, C. Wang, K. Huang, C. Yeh, A. Wang, W. Wang, M. Lin, PLOS ONE, 7(2012)e49329